View metadata, citation and similar papers at core.ac.uk

brought to you by CORE

provided by Directory of Open Access Journals

J. Min. Metall. Sect. B-Metall. 48 (3) B (2012) 449 - 459

Journal of Mining and Metallurgy, Section B: Metallurgy

SURFACE GRAIN COARSENING AND SURFACE SOFTENING DURING MACHINING OF ULTRA-FINE GRAINED TITANIUM

A.A. Symonova[a], O.N. Verezub[b], A.A. Sycheva[c,d], N.V. Verezub[a], V.L. Havin[a], G. Kaptay[d,e,*]

[a] Department of Integrated Technologies in Mechanical Engineering, National Technical University ("Kharkov Polytechnic Institute"), Kharkov, Ukraine

[b] Department of Production Engineering, University of Miskolc, Miskolc-Egyetemvaros, Hungary

[c] Materials Science Research Group, Hungarian Academy of Science-University of Miskolc, Miskolc-Egyetemvaros, Hungary

[d] Department of Nanotechnology, University of Miskolc, Miskolc-Egyetemvaros, Hungary

[e] Bay Zoltan Applied Research Nonprofit Ltd, Miskolc, Hungary

(Received 09 November 2012; accepted 25 November 2012)

Abstract

Experiments are run to show that different machining conditions applied to ultra-fine grained pure titanium lead to different levels of grain coarsening and softening near the machined surface. Under "hard" machining conditions the upper 40 microns of the machined surface are altered with a decreased microhardness. The experimental results are reasonably reproduced by model calculations. Expanding the parameter field of the model calculations, the surface coarsening diagram and the surface softening diagram due to machining are presented, showing the region of technological parameters, under which neither grain coarsening nor softening takes place along the machined surface.

Keywords: *Machining; Ultrafine grained metal; Pure titanium; Surface grain coarsening; Microhardness; Softening*

1. Introduction

The importance and practical applications of ultra-fine grained (UFG) metals increase steadily [1-2]. UFG metals and alloys can be produced by different routes, the most widely spread technology being severe plastic deformation (SPD) [3]. In this paper UFG pure titanium (Ti) is considered as a model material, as pure Ti has a great potential as an implant material, due to its biocompatibility [4]. Machining is the last and inevitable step to produce the final part from all metals, including bulk UFG metals. Thus, in this paper machining of UFG-Ti will be studied.

It is known that machining provides high local temperatures in the machined parts. It is also known that high temperatures lead to high mobility of atoms, allowing fast grain coarsening in the heat affected zone (HAZ) [5]. Thus, there is a danger that during machining of UFG metals grain coarsening will take place along the machined surface, leading to degraded properties in the HAZ [2, 6]. In ideal case such structural changes during machining should be avoided to preserve the UFG structure of the HAZ with its superior properties.

Processing of nano-grained materials was already studied in some papers [7, 8]. Change of the microstructure of UFG-Ti due to annealing was studied by [2]. However, the change of microstructure and properties along the surface of UFG-Ti during its machining has not been studied so far. To fill this gap, the following goals are set forth in this paper:

i. to use the existing databank on grain coarsening as function of time and temperature of heat treatment and on dependence of the microhardness on grain size to predict surface grain coarsening and surface softening during machining of UFG pure Ti,

ii. to carry out machining of UFG pure Ti under different machining conditions and to measure its microhardness along the machined surface and as function of depth (measured from the machined surface), with the aim to check how the experimental and theoretically predicted microhardness values agree with each other.

2. Thermal-Mechanical Modeling of Machining Induced Surface Microstructure

In this section a theoretical model is proposed to predict changes in microhardness in the HAZ of UFG pure titanium due to its machining as function of

* *Corresponding author: kaptay@hotmail.com*

DOI:10.2298/JMMB121109056S

Dedicated to the memory of Professor Zbigniew Moser

machining parameters V (cutting speed, m/min) and f (feed, mm/rev), having fixed other parameters of machining. The theory consists of the following three consecutive steps:

i. calculation of the steady-state temperature field along the machined surface of the workpiece and as function of depth (measured from the machined surface),

ii. calculation of grain coarsening as function of the duration of different temperature effects during machining,

iii. calculation of microhardness decrease (softening) as function of grain size.

In this simplified model, the above steps are not coupled. Further work is needed to couple all the modeling steps to software. We presume that this would not change the essential conclusions of this paper, although some quantitative improvement is expected if the above models are coupled in future.

2.1. Temperature field in the surface zone of the workpiece

The finite element method was used to calculate the steady state temperature field in the workpiece. During this modeling a cumulative heat source acting in grid knots was used, similar to the approach of [9-10]. The calculations were performed by the ANSYS program package [11]. The details of the calculations are given in Appendix 1. Calculations in the present paper were performed for a pure Ti sample and fixed machining conditions. The Ti-workpiece is taken as cylinder with a radius of r_w = 10 mm and a length of L_w = 100 mm. A turning tool of the hard alloy K20 (EU) was used in the calculations. The cutting conditions varied within the range of cutting speed of V = 50-200 m/min and feed of f = 0.04-0.20 mm/rev, with a constant cutting depth of d = 0.5 mm in each calculation. As an example, the calculated steady state temperature distribution is shown at V = 160 m/min and f = 0.14 mm/rev in Fig. 1. The calculated temperature distribution is shown schematically in Fig. 2.

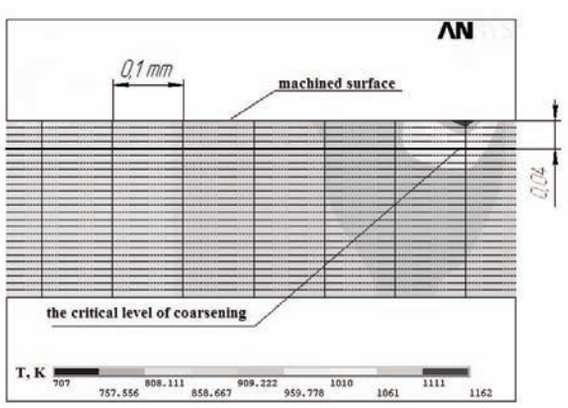

Figure 1. *A typical steady-state temperature distribution calculated for "hard" machining conditions of V = 160 m/min and f = 0.14 mm/rev (values along the scale bar correspond to temperature in K)*

One can see that the machined surface length of the workpiece at a given moment of time is divided into different sub-lengths L_i with temperature intervals $T_{i,min}$ - $T_{i,max}$ (see Fig. 2). Except the central part at i = 1, other lengths are composed of two sub-parts: $L_i = L_{ia} + L_{ib}$. The time interval t_i during which the temperature field travels a surface length of L_i can be calculated as:

$$t_i = \frac{0.12 \cdot r_w \cdot \pi \cdot L_i}{f \cdot V} \tag{1}$$

where coefficient 0.12 is used to re-calculate minutes into seconds and mm into m, multiplied by 2. As it will be shown later, the grain coarsening effect is an exponential function of temperature. That is why the weighted average temperature of interval i is calculated as:

$$T_i \cong \frac{T_{i,\min} + 2 \cdot T_{i,\max}}{3} \tag{2}$$

As an example, the calculated values of L_i, T_i and t_i are given in Table 1 for two different machining conditions. The calculated primary parameter values of Table 1 will be used in the next sub-section to calculate grain coarsening. The uncertainty of the values in Table 1 is estimated to be ± 10%.

2.2. Grain coarsening due to temperature increase

In this paper we presume that local heating during machining provides the same grain coarsening rate as that caused by heat treatment. Thus, other effects, such as pressure during machining, etc., are excluded from the analysis. Plastic shear during machining is taken into account in the calculation of the temperature field (see Appendix), and thus grain

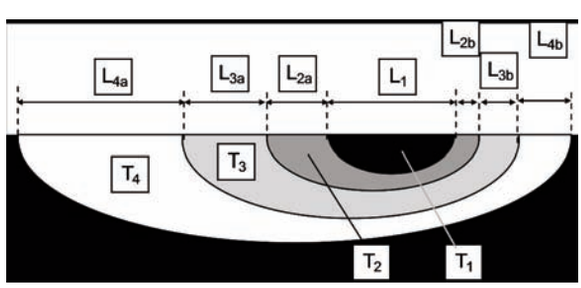

Figure 2. *Schematic of the calculated steady-state temperature distribution for a given set of machining parameters*

Table 1. *Primary parameters obtained from steady-state temperature field calculations and using Eq. (1) for the "light" and "hard" machining conditions along the surface of Ti*

f, mm/rev	V, m/min	step i	L_i, mm	t_i, s	T_i, K	z_i *, m^2	z, *, m^2	D nm
0.09	30	0	--	--	--	--	--	100
		1	0.068	0.095	696	1.0 10^{-19}	1.0 10^{-19}	100
		2	0.075	0.105	687	6.7 10^{-20}	1.7 10^{-19}	100
		3	0.2	0.279	678	1.0 10^{-19}	2.7 10^{-19}	100
		4	0.3	0.419	670	6.7 10^{-20}	3.4 10^{-19}	100
0.14	160	0	--	--	--	--	--	100
		1	0.032	0.0054	1145	4.37 10^{-14}	4.37 10^{-14}	231 ± 13
		2	0.034	0.0057	1094	1.47 10^{-14}	5.84 10^{-14}	262 ± 16
		3	0.034	0.0057	1044	4.31 10^{-15}	6.27 10^{-14}	270 ± 17
		4	0.037	0.0062	993	1.18 10^{-15}	6.39 10^{-14}	272 ± 17
		5	0.14	0.0236	943	1.00 10^{-15}	6.49 10^{-14}	274 ± 17
* parameter z_i is defined from Eq.(4.b) as: $z_i \equiv 0.3563 \cdot t_i \cdot \exp(-28061 / T_i)$, $z = \sum_i z_i$								

coarsening is also influenced by plastic shear.

When a piece of pure metal with initial grain size D_o (m) is kept at temperature T (K) during the period of time t (s), the final (coarsened) grain size D (m) can be described by the following equation [12]:

$$D \cong \sqrt{D_o^2 + k \cdot t} \tag{3.a}$$

where k is the coarsening coefficient (m^2/s). The coarsening coefficient is described by the following semi-empirical, Arrhenius type equation [12]:

$$k \cong A \cdot \exp\left(-\frac{B}{T}\right) \tag{3.b}$$

with A (m^2/s) and B (K) being semi-empirical parameters. Parameters A and B are material constants, depending on the pure metal to be heated or machined. These semi-empirical parameters can be derived from heat treatment data, without using complex machining experiments. Substituting Eq. (3.b) into Eq. (3.a):

$$D \cong \sqrt{D_o^2 + A \cdot t \cdot \exp\left(-\frac{B}{T}\right)} \tag{4}$$

Primary experimental results for pure Ti are collected in Table 2 from experiments on heat treatment. Eq. (4) can be re-arranged as:

$$y \equiv \ln\left(\frac{D^2 - D_o^2}{t}\right) = \ln A - \frac{B}{T} \tag{4.a}$$

Fig. 3 shows the data of Table 2 in accordance with Eq. (4.a). Using the mathematical form of Eq.(4.a) and the parameters of the fitted straight line in Fig. 3, the semi-empirical parameters of Eq. (4) for pure Ti follow as: A = 0.3563 m^2/s, B = 28,061 K with an uncertainty in the calculated increase of D of about 10 rel. %. It should be mentioned that during this parameter evaluation the results of short-time experiments [2] were not taken into account (see empty circles in Fig.2).

Table 2. *Summary of heat treatment – grain coarsening experiments for pure Ti*

D_o, nm	t, s	T, K	D, nm	Source	k (Eq.3a), m^2/s
100	18,000	693	150	[3]	6.9 10^{-19}
100	10,800	773	1,000	[13]	9.2 10^{-17}
400	600	773	800	[2]	8.0 10^{-16}
400	600	823	2,300	[2]	8.6 10^{-15}
400	600	873	3,100	[2]	1.6 10^{-14}
100	1,800	1,073	50,000	[14]	1.4 10^{-12}

Table 2 is also used by us to perform our model calculations for the initial grain size of about 100 nm, as SPD procedures, being similar to our procedure leading to this approximated grain size.

If the calculated values L_i, t_i and T_i are known for different intervals from the finite element calculation of the temperature field (see Table 1), Eq. (4) can be applied in the following form to estimate the final grain size (the same equation serves as definition of z):

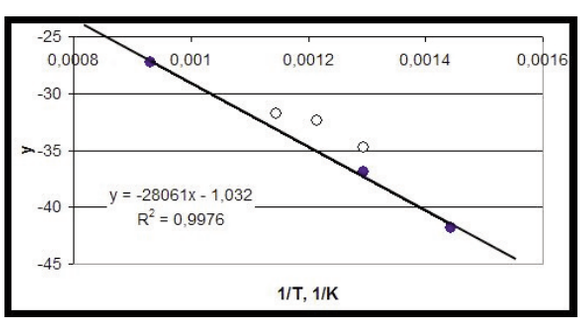

Figure 3. *The plot in accordance with Eq. (4.a) using the data of Table 2*

$$D \cong \sqrt{D_o^2 + A \cdot \sum_i t_i \cdot \exp\left(-\frac{B}{T_i}\right)} \equiv \sqrt{D_o^2 + z} \qquad (4.b)$$

The results of calculations performed by Eq. (4.b) using the data of Table 1 are shown in the last columns of Table 1 and in Fig. 4, supposing that the initial grain size is 100 nm. Fig. 4 shows a clear difference between "hard" machining conditions (V = 160 m/min, f = 0.14 mm/rev) leading to considerable grain coarsening and "light" machining conditions (V = 30 m/min, f = 0.09 mm/rev), leading to no grain coarsening, at all. This example shows that using certain sets of "light enough" machining parameters the UFG structure of the machined surface can be preserved.

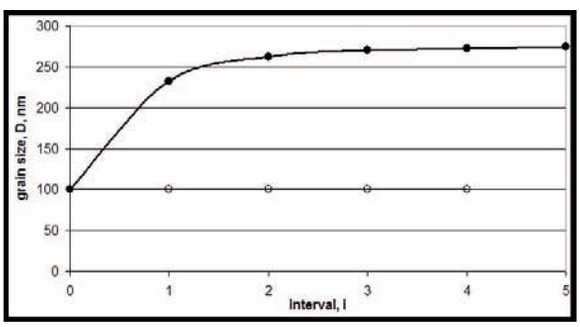

Figure 4. *Results calculated by Eq. (4.b) with D_o = 100 nm. Full symbols correspond to "hard" machining conditions: V = 160 m/min, f = 0.14 mm/rev, empty symbols correspond to "light" machining conditions: V = 30 m/min, f = 0.09 mm/rev (see Table 1.)*

One can also see from Fig. 4 that only the first 4 intervals with highest temperatures provide significant influence on the final grain size. As the T-step is 4.5% (in K-scale, see Table 1 for "hard" conditions), one can conclude that considering only the highest 18% (in K-scale) of the T-interval is sufficient to obtain a reasonably correct calculated value for the final grain size. Lower temperatures have negligible effect due to the exponential T-dependence of Eq. (4.b).

For the "hard" machining conditions, the above procedure was repeated with the calculated T-distribution at different depths below the machined surface (Fig-s. 1, 5). One can see that the grain size decreases rapidly as function of depth below the machined surface. Particularly, the grain size decreases from 274 ± 17 nm (surface value) to 121 ± 2 nm (value at a depth of 40 μm), compared to its initial value of 100 nm. Thus, coarsening at a depth of 40 μm below the machined surface becomes quite small (around 20%).

The simulation of the T-field (see Fig. 1) during machining of pure Ti and calculations by Eq. (4.b)

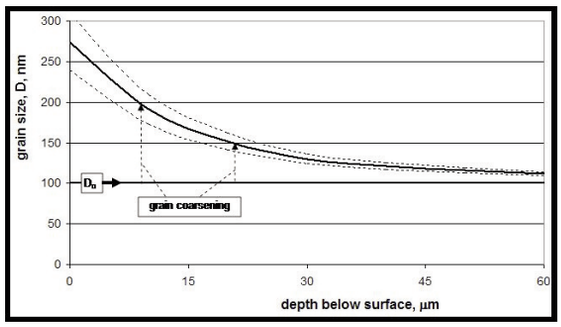

Figure 5. *Grain size calculated by Eq. (4.b) and Figure 1 as function of depth from the machined surface (parameters: V = 160 m/min, f = 0.14 mm/rev)*

were extended to parameter intervals of V = 50-200 m/min and f = 0.04-0.20 mm/rev. The following approximated equation is found for parameter z of Eq.(4.b):

$$\ln z \cong -47 + 0.041 \cdot V + (38 + 0.18 \cdot V) \cdot f \qquad (5.a)$$

The agreement between the simulated by Eq.(4.b) and approximated by Eq.(5.a) values of parameter ln$z$ is demonstrated in Fig. 6. The agreement is satisfactory for the demonstrational purposes of this paper.

From Eq-s. (4.b, 5.a), the critical value of f can be expressed, causing the certain grain size D as function of D_o and V:

$$f_{cr,coars} = \frac{\ln\left(D^2 - D_o^2\right) + 47 - 0.041 \cdot V}{38 + 0.18 \cdot V} \qquad (5.b)$$

Eq. (5.b) can be specified to calculate the critical f-values for D_o = 100 nm and for D = 110 nm (= 10% grain coarsening) or D = 200 nm (= 100% grain coarsening):

$$f_{cr,coars10\%} = \frac{13.2 - 0.041 \cdot V}{38 + 0.18 \cdot V} \qquad (5.c)$$

$$f_{cr,coars100\%} = \frac{15.9 - 0.041 \cdot V}{38 + 0.18 \cdot V} \qquad (5.d)$$

Eq-s (5.c-d) are used to construct the surface grain coarsening diagram in Fig. 7. Based on Fig. 7, machining conditions can be selected to ensure that no significant grain coarsening takes place during

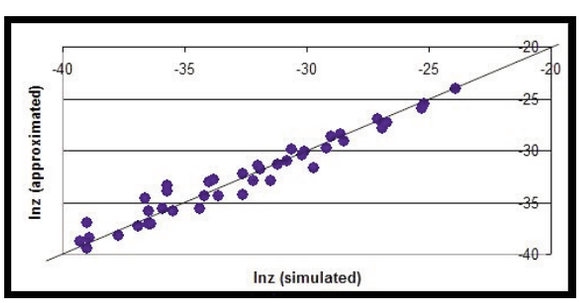

Figure 6. *Comparison of simulated by Eq.(4.b) and approximated by Eq.(5.a) values of parameter lnz*

machining along the machined surface. Although Fig. 7 is valid only for specific conditions (pure Ti, D_o = 100 nm, d = 0.5 mm, d_w = 20 mm, tool K20), similar diagrams can be constructed for other metals and other machining parameters using the algorithm of calculation developed above.

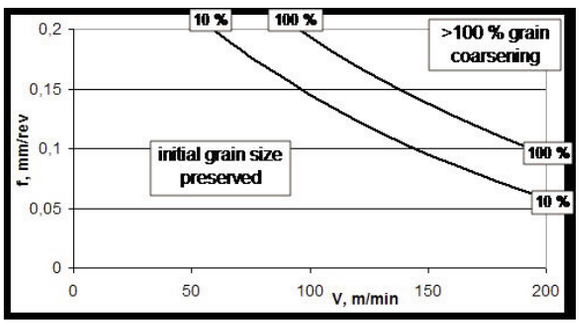

Figure 7. *The surface grain coarsening diagram of pure Ti due to machining showing different regions of technological parameters (V and f) (valid for D_o = 100 nm, d = 0.5 mm, r_w = 10 mm, tool K20)*

2.3. Decrease in surface microhardness due to grain coarsening

It is widely known that mechanical properties of UFG metals gradually degrade as grain size is increased. The well-known Hall-Petch equation [15] is applied for the grain size dependence of microhardness:

$$HV = HV_o + \frac{k_{HV}}{\sqrt{D}} \quad (6)$$

where HV is microhardness (MPa) of the UFG sample of the given grain size (D, m), while HV_o (MPa) and k_{HV} (MPa $m^{0.5}$) are semi-empirical parameters, being different for each pure metal at a given temperature. The experimental data for Ti and other metals [16-18] are shown in Fig. 8, measured at room temperature. Fig. 8 proves that Eq. (6) describes the experimental data reasonably well, with values of R^2 being 0.856 for Ti, 0.989 for Ni and 0.995 for Nb. We also show our data points (for details see below) for macro-grained (1800 MPa) and UFG (2800 MPa) titanium. One can see that these data agree quite well with the data of Valiev and Aleksandrov [16]. As data of [16] deviate from the linear trend in Fig. 8 in the medium interval of grain sizes (especially if compared to data obtained for Ni and Nb), the following parameters of Eq. (6) are taken in this paper, estimated through our two measured points: HV_o = 1690 MPa, k_{HV} = 0.351 MPa $m^{0.5}$ with an uncertainty in the calculated HV value of ± 10% (see dotted line in Fig. 8).

The results of trial calculations by Eq. (6) for microhardness are shown in Table 3. One can see that under light machining conditions both the grain size

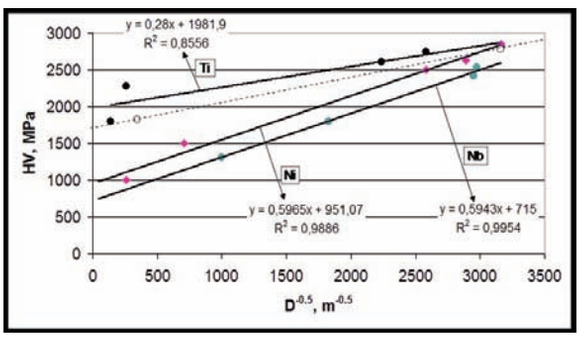

Figure 8. *The grain size dependence of the microhardness of some UFG pure metals. Data are taken from Valiev and Aleksandrov [16] for Ti, from Pimogin et al. [17] for Ni and from Popova [18] for Nb. Empty points show our measured data for the initial (macro-grained) Ti and for the UFG Ti.*

and microhardness remain unaffected. On the other hand, under hard machining conditions the initial surface grain size increases by a factor of 2.74, while the initial surface microhardness decreases by about 16%.

Table 3. *Calculated surface grain size and surface microhardness of pure Ti machined under different conditions*

Machining conditions	f, mm/rev	V, m/min	D, nm	HV, MPa
None	--	--	100	2800
Light	0.09	30	100	2800
Hard	0.14	160	274	2360

In Fig. 9, the microhardness values calculated by Eq. (6) as function of depth below the machined surface are shown for hard machining conditions, being in agreement with Fig. 5. One can see from Fig. 9 that at a depth of 40 μm below the machined surface softening becomes negligible (about 3.5% of the

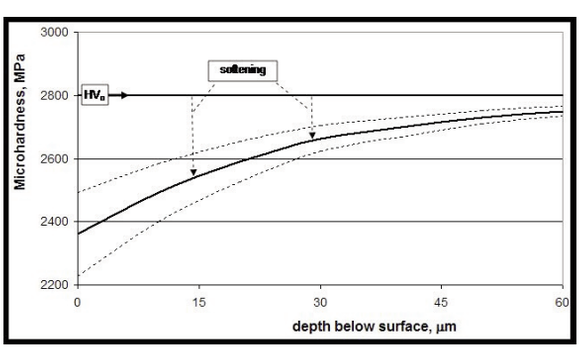

Figure 9. *Dependence of microhardness on the depth below the machined surface. Calculated from the data of Figure 5, using Eq. (6)*

initial value of the un-machined part).

Substituting Eq. (5.a) into Eq. (6), the critical value of f can be expressed, causing a certain softening, i.e. leading to a given HV microhardness value as function of D_o and V:

$$f_{cr,soft} = \frac{\ln\left[\left(\frac{0.351}{HV-1690}\right)^4 - D_o^2\right] + 47 - 0.041\cdot V}{38 + 0.18\cdot V} \quad (7.a)$$

Eq. (7.a) can be used to calculate the critical f-values for D_o = 100 nm and for HV = 2660 MPa (= 5% softening compared to 2800 MPa) or HV = 2240 MPa (= 20% softening compared to 2800 MPa):

$$f_{cr,soft5\%} = \frac{14.4 - 0.041\cdot V}{38 + 0.18\cdot V} \quad (7.b)$$

$$f_{cr,soft20\%} = \frac{17.5 - 0.041\cdot V}{38 + 0.18\cdot V} \quad (7.c)$$

Eq-s (7.b-c) are used to construct the surface softening diagram in Fig. 10. Based on Fig. 10, machining conditions can be selected to ensure that no significant softening takes place during machining along the machined surface. Although Fig. 10 is valid only for specific conditions (pure Ti, D_o = 100 nm, d = 0.5 mm, r_w = 10 mm, tool K20), similar diagrams can be constructed for other metals and other machining parameters using the algorithm of calculation developed above.

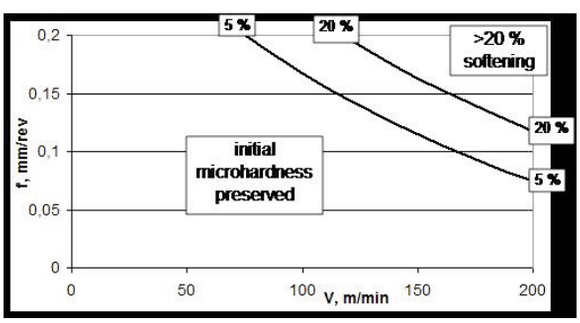

Figure 10. *The surface softening diagram of pure Ti due to machining showing different regions of technological parameters (V and f) (valid for D_o = 100 nm, d = 0.5 mm, r_w = 10 mm, tool K20)*

2.4. Summary of the theoretical part

The above theory/algorithm is proposed as a tool to predict the range of machining parameters under which pure UFG metals can be machined without a danger of softening the machined surface. Particularly, Fig. 10 is proposed as an approximated softening diagram for pure Ti under conditions given above.

Later in this paper, experiments will be described to produce UFG pure Ti, machine it under different conditions and measure its micro-hardness along the machined surface and below it as function of depth. The final results of the above theory presented in Figs 9-10 will be compared to the experimental results. In case of a relatively good agreement, the above theory and calculation algorithm for surface softening will be taken as proven, at least in the first approximation.

3. Design of the experimental verification of the theory

Technically pure titanium of grade T (EU) of the following chemical composition has been used in the experiments (weight %, max.): 0.07 C, 0.18 Fe, 0.12 O, 0.03 N, 0.01 H, with the titanium content being not less than 99.5%. The starting Ti-samples (hereinafter referred to as "macro Ti") are cold-rolled sticks having a macro-crystalline structure with an average grain size of about 10 microns.

Multiple forging as one of the possible ways of severe plastic deformation (SPD) was used to obtain UFG structured high-strength titanium. This method includes multiple repetitions of free forging (for details see [13]). The process was carried out at a temperature of the sample of 773 K in an induction furnace. After four passes including operations of setting-drawing, the sample was cooled in dry sand. Bulk homogeneous titanium was obtained after this operation. Hereinafter, this sample is referred to as "UFG-Ti".

Samples "macro-Ti" and "UFG-Ti" were used as workpieces in machining experiments with a diameter of r_w = 10 mm and a length of L_w = 100 mm. A turning tool of the hard alloy K20 (EU, composition: 8% Co, 92% WC) was used for the machining experiments. The geometric parameters of the cutting part of the tool were as follows: cutting angle γ = 0º, back angle α = 10º, frontal approach angle φ = 45º, cutting edge inclination angle λ = 0º, radius of nose curvature – 0.5 mm. The cutting conditions varied within the range of V = 30-160 m/min, f = 0.09-0.2 mm/revolution with a constant cutting depth of d = 0.5 mm in each machining experiment. No lubricant or coolant was used for the experiments.

The average temperature in the cutting zone was measured by the thermal electromotive force at the tool-chip interface, which acts as a hot junction between the two materials (tool and chip) of different compositions (for details, see [19]). In order to convert the mV values of working millivoltmeter to degrees of Kelvin, the instrument is calibrated by a natural thermocouple. Aluminum bath is used for this purpose. As the bath heats up and cools down, its temperature is registered periodically by a control thermocouple. Simultaneously, thermal emf of the natural thermocouple is registered by the working millivoltmeter. Based on the obtained data, a calibration graph is plotted. Knowing the values of thermal emf, it is possible to calculate the values of

temperature from the calibration graph. The temperature in the heat affected surface zone of the workpiece is approximately equal to the temperature measured this way. The calculated maximum surface temperature (see Appendix 1) agreed within 15% with these measured values, confirming the approximated validity of both experimental and calculated temperature values.

The roughness of the machined workpiece surfaces was measured using standard techniques with an electron profilograph-profilometer model "Sartronic3+". To obtain reliable experimental results, the measurement was repeated 4-5 times. The relative uncertainty of the measurement did not exceed 10%.

The microhardness of the sample was measured with a load of 0.49 N as function of depth measured from the machined surface by a "Carl Zeiss, Jena, Mikrohaterprüfer Hanemann" setup equipped with a Vickers pyramid. The microhardness measurements were repeated 9-10 times, and their relative uncertainty did not exceed 10%.

4. Results and evaluation

The influence of cutting speed on the temperature in the cutting zone is shown in Fig. 11. It is in agreement with the summary by Trent and Wright [20], showing that high cutting speeds lead to increased temperature in the HAZ. As one can see from Fig. 11, the measured maximum temperature in the HAZ during machining is always higher for UFG-Ti compared to macro-Ti. The reason is that UFG-Ti has a higher hardness and thus a higher resistance to machining.

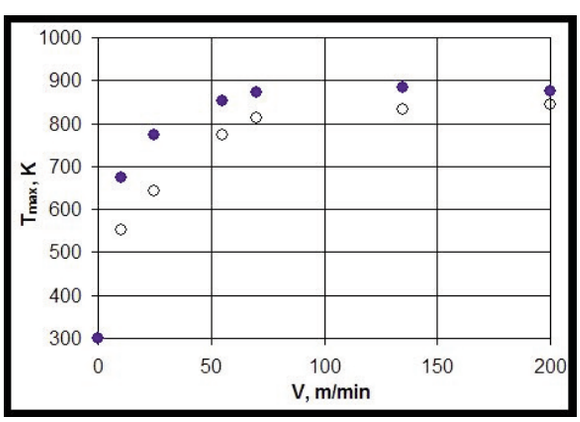

Figure 11. *The measured maximum temperature in the HAZ as function of cutting speed for "macro-Ti" (empty symbols) and "UFG-Ti" (full symbols) (f = 0.1 mm/rev)*

The temperature difference shown in Fig. 11 gradually decreases with increasing the cutting speed and temperature (see Fig. 12). This is probably due to the in-situ softening of the UFG-Ti during machining with increasing temperature.

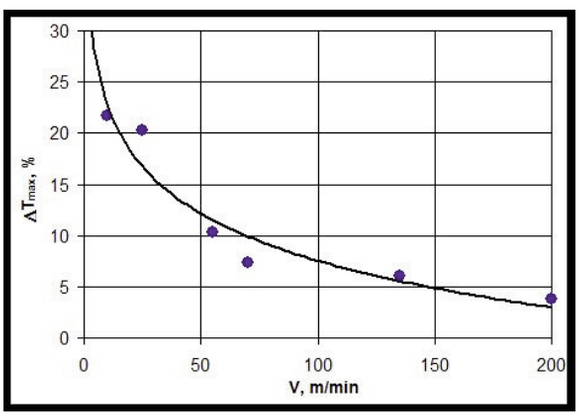

Figure 12. *The relative increase of measured maximum temperature in the HAZ for the UFG-Ti compared to that in the macro-Ti as function of cutting speed (f = 0.1 mm/rev)*

The influence of machining parameters on grain coarsening can be judged from the measured roughness of the UFG-Ti samples after machining. When machining is performed under "light" conditions (with f = 0.09 mm/rev), surface roughness does not considerably increase with increasing the machining speed, V (see Fig. 13). However, under "hard" machining conditions (with f = 0.14 mm/rev), the roughness increases considerably with increasing the machining speed, V, and has a considerably higher absolute value compared to that obtained under "light" machining conditions.

Finally, let us show how machining influences the micro-hardness of the surface layer. The initial "macro-Ti" sample has a microhardness of 1800 MPa. The UFG-Ti sample has a considerably increased microhardness of about 2800 MPa compared to

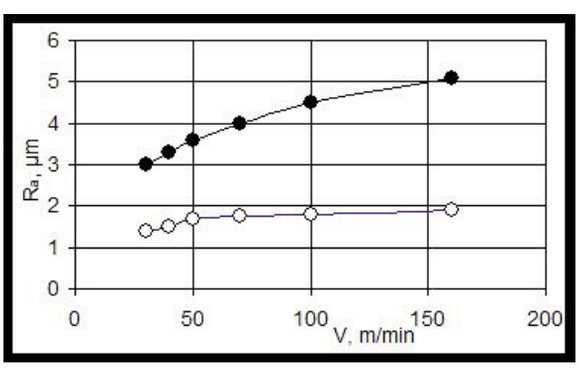

Figure 13. *Dependence of roughness of the machined UFG-Ti on cutting parameters (empty symbols: f = 0.09 mm/rev, full symbols: f = 0.14 mm/rev)*

macro-Ti, which agrees well with the literature values [16, 21]. During machining the microhardness of the UFG-Ti sample decreases. For the "hard" machining conditions (V = 160 mm/min, f = 0.14 mm/rev) the microhardness is shown in Fig. 14 as function of depth measured from the machined surface. One can see that at a depth of 40 microns and below the microhardness is not influenced considerably by machining and has a value close to that of the non-machined UFG-Ti sample. Thus, we can conclude that machining under "hard" conditions degrades the properties of the surface layer of pure UFG-Ti to a depth of 40 microns. From the comparison with Fig. 9 (see lines in Fig. 14), we can conclude that the agreement between the experimental and calculated values is reasonable.

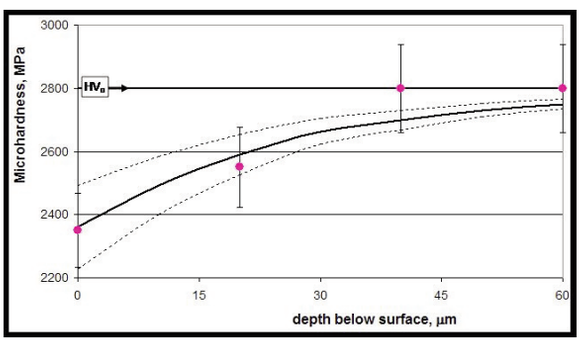

Figure 14. *Dependence of microhardness of the UFG-Ti machined sample on the depth measured from the machined surface (V = 160 mm/min, f = 0.14 mm/rev). Points: measured values, lines are imported from Figure 8*

The softening diagram Fig. 10 is repeated with two measured points in Fig. 15. One can see that the experimental points are positioned in reasonable theoretical regions of the surface softening diagram.

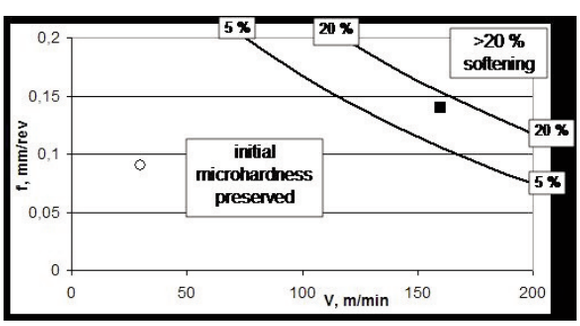

Figure 15. *The surface softening diagram of pure Ti due to machining showing different regions of technological parameters (V and f) (valid for D_o = 100 nm) (copy of Figure 9). Full point: experiment under hard conditions, resulting in 16% softening. Empty point: experiment under light machining conditions, resulting in negligible softening*

Thus, the theory developed above is confirmed, at least, in the first approximation. We consider our results only as a preliminary indication that machining can lead to surface softening of UFG metals. Much more work is needed both experimentally and theoretically to extend the findings of the present paper.

5. Conclusions

It is demonstrated experimentally that during machining of pure UFG Ti, a temperature increase leads to softening of the machined surface under "hard" machining conditions.

A model is developed to predict surface softening of UFG pure metals due to machining. The model consists of i) a finite element calculation of the steady state temperature field in the workpiece, ii) the equation linking grain coarsening with temperature and time duration of its action and iii) the equation linking microhardness with grain size. A surface grain coarsening diagram and a surface softening diagram are plotted for pure UFG Ti with an initial grain size of 100 nm. The diagrams can be used to select technological parameters of machining (speed and feed) that ensure no surface softening during machining.

The experimental measurements are found to be in reasonable agreement with the surface softening diagram. Thus, the principle and algorithm to construct surface softening diagrams are confirmed in the first approximation.

Acknowledgement

This work is based on the scientific and contractual work (No.010U001236) and is financed partly by the program Ministry of the Education and Science of Ukraine in the National Technical University "Kharkov Polytechnic Institute", and partly by TAMOP-4.2.1.B-10/2/KONV-2010-0001 project with support by the European Union and the European Social Fund. The help of dr. Jaroslav Sytchev in the preparation of this manuscript is appreciated.

References

[1] G. Hornyak, J. Dutta, H. Tibbals, A. Rao, Introduction to Nanoscience. CRC Press, New York, 2008.

[2] M. Hoseini, M.H. Pourian, F. Bridier, H. Vali, J.A. Szpunar, P. Bocher, Mater. Sci. Eng. A 532 (2012) 58-63.

[3] R.Z. Valiev, Nature Mater. 3 (2004) 511-516.

[4] V. Latysh, G. Krallics, I. Alexandrov, A. Fodor, Current Appl. Phys., 6 (2006) 262-266.

[5] D. Priadi, R.A.M. Napitupulu, E.S. Saradj: J. Min. Metall. Sect. B-Metall. 47 (2) B (2011) 199 – 209.

[6] Y. Karpat , J. Mater. Process. Technol, 211 (2011) 737-749.

[7] R. S. Averback, H. J. Höfler, R. Tao, Mater. Sci. Eng. A 166 (1993) 169–177.
[8] R.Y. Lutfullin, A.A. Kruglov, R.V. Safiullin, M.K. Mukhametrakhimov, O.A. Rudenko, Mater. Sci. Eng. A 503 (2009) 52-54.
[9] H. Chandrasekaran, A. Thuvander, Machin. Sci. Technol. 2 (1998) 355-367.
[10] A. Bareggi, G.E. O'Donnell, A. Torrance, Proceedings of the 24th International Manufacturing Conference, Waterford, 1 (2007) 263-272.
[11] ANSYS Basic Analyzes Procedure Guide. ANSYS Release 5.6., ANSYS Inc. 1998.
[12] J. Geiger, A. Roosz, P. Barkoczy, Acta Mater. 49 (2001) 623-629.
[13] G.A. Salishchev, S.P. Malisheva, R.M. Galeyev, FMM 82 (1996) 117-127.
[14] K. Inyoung, J. Won-Sik, K. Jongyoul, P. Kyung-Tae, H.S. Dong, H.S., Scripta Mater. 45 (2001) 575-581.
[15] J.D. Verhoeven, Fundamentals of physical metallurgy, John Wiley, NY. 1975.
[16] R.Y. Valiev, I.V. Aleksandrov, Nanosturctured metals obtained by SPD (in Russian), Logos, Moscow, 2000.
[17] V.P. Pimogin, T.M. Gaponceva, T.I. Chashuchina, L.M. Voronova, FMM 105 (2008) 438-445.
[18] E.N. Popova, FMM 103 (2007) 426-432.
[19] Kalpakjian, S., 1995. Manufacturing Engineering and technology, Addison-Wesley Publ. Comp., Amsterdam (see page 614).
[20] Trent, E.M., Wright, P.K., 2000. Metal cutting. Butterworth – Heinemann, New-York, pp. 446.
[21] V.V. Stolyarov, Y.T. Zhu, T.C. Lowe, R.Z. Valiev, Mater Sci Eng A, 303 (2001) 82-89.
[22] A.N. Reznikov, Thermophysics of cutting (in Russian), Mashinostroenie, Moscow, USSR, 1969.
[23] M.F. Poletika, Contact phenomena at metal cutting (in Russian), Izv. Tomskogo Polytech. Inst., Tomsk, USSR, 1965.
[24] D.R. Poirier, G.H. Geiger, Transport Phenomena in Materials Processing, TMS, Warrendale, USA, 1994.
[25] Yu. Altintas. Manufacturing Automation: Metal Cutting Mechanics, Machine Tool Vibrations and CNC Design, Cambridge, Cambridge University Press, 2000.
[26] J. Emsley, The Elements - Clarendon Press, Oxford, UK, 1989.
[27] A.A. Nazarov, A.E. Romanov, R.Z. Valiev, Acta Metall Mater, 41 (1993) 1033-1040.

Appendix

Calculation of the temperature field during machining of a cylindrical workpiece

Let us consider a cylindrical workpiece of radius r_w (mm) and length L_w (mm), studied in cylindrical coordinates r (radius) and z (length along the axis starting from the left end). The material of the workpiece is characterized by its thermal diffusivity, α_w (m^2/s). The workpiece is being machined from the right to the left (Fig. A1) at a cutting depth of d (mm) using frontal approach angle of the tool φ (the tool is not shown in Fig. A1). Machining is performed at a speed of V (m/min) along the perimeter of the cylinder and a feed of f (mm/rev) along direction z. The major elements of the calculation algorithm given below have been worked out in [22-23].

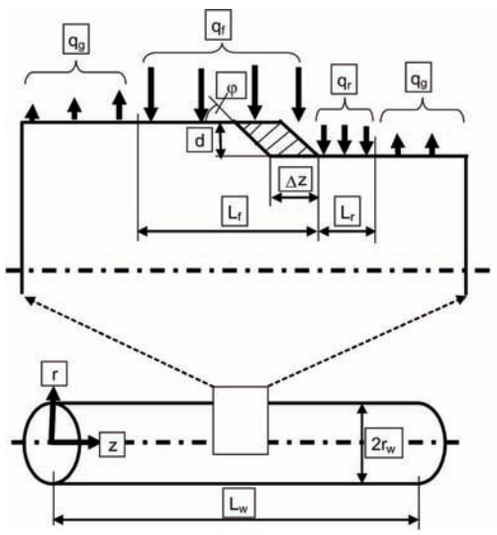

Figure A1. *Schematic of a cylindrical workpiece in the z-r coordinate system and the heat flow densities (q_f = incoming heat density in front of the tool, q_r = incoming heat density behind the tool, q_g = heat loss density to the convective gas, the dashed area is removed during step Δz)*

The rotational frequency of the cylinder is: $n = 1000 \cdot V / (2 \cdot r_w \cdot \pi)$ (1/min). The velocity in the z direction is: $V_z = f \cdot n / 1000 = f \cdot V / (2 \cdot r_w \cdot \pi)$ (m/min).Thus, the ratio of the two speeds: $V / V_z = 2 \cdot r_w \cdot \pi / f$. If r_w = 2.5 mm, f < 0.2 mm/rev, then V/V_z > 78. Thus, the speed along the perimeter is higher than that along the z direction by about 2 orders of magnitude. Therefore, heat flow densities along the contact of the workpiece with the tool will be considered as constant along the contact lengths L_f and L_r (m), i.e. in front of and in the rear of (behind) the tool (see Fig. A1). The rear contact length, L_r, is taken equal to the flank wear width of the tool and equals 0.1 mm [22]. The front contact length is calculated from the semi-empirical equation of the same author as:

$$L_f \cong (2.05 \cdot r_c - 0.55) \cdot f \cdot \sin\phi \qquad \text{(A1)}$$

where r_c is the chip thinning ratio (dimensionless), with an average value of r_c = 1.1.

The following general equation is used in cylindrical coordinates [24] to describe the temperature field within the workpiece:

$$\frac{\partial T}{\partial t} = \alpha_w \cdot \left[\frac{1}{r} \cdot \frac{\partial \left(r \cdot \frac{\partial T}{\partial r} \right)}{\partial r} + \frac{\partial^2 T}{\partial z^2} \right] \qquad \text{(A2)}$$

where T is temperature (K), t is time (s). The starting condition is: $T(r,z,0) = T_o$. The boundary conditions are:

if z is within L_f: $\lambda_w \cdot \frac{\partial T(r_w,z,t)}{\partial r} = q_f$ (A3.a)

if z is within L_r: $\lambda_w \cdot \frac{\partial T(r_w,z,t)}{\partial r} = q_r$ (A3.b)

if z is outside of both L_f and L_r:

$$\lambda_w \cdot \frac{\partial T(r_w,z,t)}{\partial r} = h \cdot \left[T_g - T(r_w,z,t)\right] \quad \text{(A3.c)}$$

along the centerline of the workpiece:

$$\frac{\partial T(0,z,t)}{\partial r} = 0 \quad \text{(A3.d)}$$

at the left end of the cylinder:

$$\lambda_w \cdot \frac{\partial T(r,0,t)}{\partial z} = h \cdot \left[T(r,0,t) - T_g\right] \quad \text{(A3.e)}$$

at the right end of the cylinder:

$$\lambda_w \cdot \frac{\partial T(r,L_w,t)}{\partial z} = h \cdot \left[T_g - T(r,L_w,t)\right] \quad \text{(A3.f)}$$

where λ_w (W/mK) is the heat conductivity of the workpiece, q_f (W/m^2) and q_r (W/m^2) are heat flow densities along lengths L_f and L_r (see above) respectively (when the heat flow density is positive, its vector is directed towards the workpiece), h (W/m^{2}K) is the heat transfer coefficient along the surface of the workpiece in contact with gas, T_g (K) is the temperature of gas far from the workpiece. In the first approximation, the heat transfer coefficient is taken as constant along the whole surface area of the workpiece, except the circumferences denoted by L_f and L_r.

Since in this formulation the thermally deformed state of the workpiece during turning is of interest to us, while the temperature field in the vicinity of the cutting edge (cutting temperature) is not the goal of calculation, the distribution of heat source can be considered uniform with reasonable accuracy and its intensity can be determined by the following dependencies. The heat flow density along the rare surface (length of L_r) can be approximately written as:

$$q_r \cong 0.10 \cdot \sigma \cdot V \quad \text{(A4)}$$

where σ is the tensile strength of the machined material (Pa). The heat flow density along the front surface (length of L_f) consists of two terms, due to the uniformly distributed friction source (q_{uf}) and due to the heat released during plastic shear of the chip formation zone (q_d):

$$q_f = q_{uf} + q_d \quad \text{(A5)}$$

The heat flow density along the front surface, due to the uniformly distributed friction force is written as:

$$q_{uf} = \frac{\left[\left(F_t - F_u\right) \cdot \sin\gamma + \left(F_n - F_v\right) \cdot \cos\gamma\right] \cdot V}{L_f \cdot b \cdot r_c \cdot 60} \quad \text{(A6)}$$

where γ is the tool's rake angle, b is the cut width (m): $b = d/\sin\varphi$. The tangential (F_t, N) and the normal components of the cutting force (F_n, N), the normal longitudinal force (F_v, N) and the frictional force (F_u, N) acting on the rear surface of contact between the tool and the workpiece are written as [25]:

$$F_t \cong 360 \cdot d^{0,7} \cdot f^{0,58} \cdot V^{0,2} \quad \text{(A7.a)}$$

$$F_n \cong 0.4 \cdot F_t \quad \text{(A7.b)}$$

$$F_v = F \cdot \cos^2{}_a \quad \text{(A7.c)}$$

$$F_u = F \cdot \sin^2{}_a \quad \text{(A7.d)}$$

where F is the resulting cutting force (N):

$$F = \sqrt{F_t^2 + F_f^2} \quad \text{(A7.e)}$$

where F_f is the feed force (N):

$$F_f \cong 166 \cdot d^{1,2} \cdot f^{0,3} \cdot V^{0,2} \quad \text{(A7.f)}$$

The quantity β_α of Eq-s (A9-10) is the friction angle, calculated as:

$$^2{}_a = \gamma + \tan^{-1}\frac{F_f}{F_t} \quad \text{(A8)}$$

The approximated Eq-s (A7.a, b, f) are obtained based on experimentally measured values of the components of the cutting force by dynamometer "Kistler", using hard alloy K20 and applying the analytical expressions of Trent [20].

The heat flow density along the front surface due to plastic shear of the chip formation zone is written as:

$$q_d = \left[\left(F_t - F_u\right) \cdot \left(r_c - \sin\gamma\right) - \left(F_n - F_v\right) \cdot \cos\gamma\right] \cdot \frac{V \cdot \sin\beta_1}{a \cdot b \cdot r_c} \quad \text{(A9)}$$

where a is the cutting thickness (m): $a = f \cdot \sin\phi$, while β_1 is the shear angle:

$$\sin\beta_1 = \frac{\cos\gamma}{\sqrt{r_c^2 - 2 \cdot r_c \cdot \sin\gamma + 1}} \quad \text{(A10)}$$

The heat transfer coefficient is calculated from the following equation:

$$h \cong k_H \cdot \frac{\lambda_g}{2 \cdot r_w} \cdot \mathrm{Re}^n \quad \text{(A11.a)}$$

where Re is the Reynolds number, defined as:

$$\mathrm{Re} \equiv \frac{2 \cdot r_w \cdot V}{\nu_g} \quad \text{(A11.b)}$$

where k_H and n are dimensionless semi-empirical parameters, λ_g (W/mK) and υ_g (m^2/s) are thermal conductivity and kinematic viscosity of the gas at T_g (if $500 < Re < 1000$, then: $k_H = 0.43$, $n = 0.5$, while if $1000 < \mathrm{Re} < 20{,}000$, then $k_H = 0.216$, $n = 0.6$ [22].

The finite element program is stopped in the middle of the 3rd run of machining, i.e. after the tool traveled a path of $2.5L_w$ along direction z from the right to the left. In between the cutting runs the tool returns to its original position without cutting. During this short time the workpiece cools a little, but anyhow, the consecutive cutting runs gradually increase the temperature of the workpiece. After the first 3 cutting runs steady state is reached, i.e. the

temperature fields obtained after $2.5L_w$ and after $3.5L_w$ of machining path along direction z do not differ significantly. An example of calculation results is shown in Fig. 1. The constant parameters used for the calculations are: radius of workpiece: r_w = 10 mm, length of workpiece: L_w = 100 mm, N = 1000, heat conductivity of workpiece (Ti): λ_w = 21.9 W/mK, thermal diffusivity of workpiece: α_w = 9.2 mm^2/s [26], tensile strength of the workpiece: σ=650 MPa [27], starting and gas temperature: $T_o = T_g$ = 291 K, thermal conductivity of gas: λ_g = 0.026 W/mK, kinematic viscosity of gas at T_g: υ_g = 15 mm^2/s [24], tool material: hard alloy K20, rake angle γ = 0º, frontal approach angle of the tool: φ = 45º, cutting depth: d = 0.5 mm. The front and rear lengths of contact (L_f and L_r) are calculated; while the front and rear heat flow densities (q_f, q_r) are calculated in accordance with the above algorithms. Different runs were performed with varying systematically the cutting speed (V = 30-160 m/min) and feed (f = 0.09-0.2 mm/rev). The result of calculations at V = 160 m/min and f = 0.09 mm/rev is presented in Fig. 1.

The number of elements is 750, while the number of knots is 806. Along direction z the knots are separated at a distance of Δz, obtained as $\Delta z = L_w / N$ (where N is the number of knots along direction z). The distance between the knots in direction r is 10% of Δz ($\Delta r = 0.1\ \Delta z$). The time step Δt, during which the tool travels a distance of Δz is calculated from the velocity in the z direction, $V_z = f \cdot V / (2 \cdot r_w \cdot \pi)$ and definition, as: $V_z \equiv \Delta z / \Delta t$

$$\Delta t = \frac{120 \cdot \pi \cdot r_w}{f \cdot V} \cdot \Delta z \qquad \text{(A12)}$$

The heat conducting finite element ‘PLANE55 2-D Thermal Solid’ was chosen from the ANSYS program. PLANE 55 can be used as a plane element or as an axisymmetric ring element with a two-dimensional thermal conduction capability. The element has four nodes with a single degree of freedom (temperature) at each node. The element is applicable to two-dimensional, steady-state or transient thermal analysis.